Luminescence properties of a solid solution typed $(Ba,Ca)_3MgSi_2O_8$: Eu^{2+}, Mn^{2+} phosphor with a 660 nm-featured photosynthetic action spectrum*

SONG Jun (宋俊)[1], **SUN Liang** (孙亮)[2], **LI Jian** (李建)[1], **MA Jian** (马健)[2], **and WANG Da-jian** (王达健)[1,2,3]**

1. Institute of Materials Physics, Tianjin University of Technology, Tianjin 300384, China

2. Tianjin Key Laboratory for Photoelectronic Materials and Devices, Tianjin University of Technology, Tianjin 300384, China

3. Key Laboratory of Display Materials and Photoelectronic Devices, Ministry of Education, Tianjin University of Technology, Tianjin 300384, China

(Received 7 April 2014)

A solid-solution-phase $Ba_{1.75}Ca_{1.25}MgSi_2O_8$: Eu^{2+}, Mn^{2+} phosphor in the photosynthetic action spectrum with dual band emissions at 438 nm and 660 nm is fabricated. X-ray diffraction (XRD) confirms the presence of the solid-solution phase. With the supporting information from the diffuse reflection spectrum, a feasible way to obtain higher energy-transfer (ET) efficiency is attained, and the ET efficiency of Eu^{2+}–Mn^{2+} is enhanced to 76%. The mechanism of this enhancement is owing to variation of the solid solution composition of $Ca_3MgSi_2O_8$ and $Ba_3MgSi_2O_8$, which contributes to the extension of the critical distance. Temperature-dependent results show an enhancement which is attributed to Ca. These enhancements show great promise for improving eco-lighting devices.

Document code: A **Article ID:** 1673-1905(2014)05-0343-4

DOI 10.1007/s11801-014-4055-1

In recent years, phosphors with dual band emissions of blue (400–500 nm) and red (620–680 nm, 720–740 nm) light have attracted much attention owing to their superior features in response to photosynthesis[1], especially for phosphors whose emission spectra could match the photosynthetic action spectrum (PAS). There have been many attempts to fabricate these phosphors with specific spectra, for example, Ce^{3+}/Eu^{2+} and Mn^{2+}[2-4], Gd^{3+} and Ce^{3+}[5], Ce^{3+} and Tb^{3+}[6], Er^{3+} and Yb^{3+}, etc[7]. It is well known that the luminescent efficiency of d→f electric-dipole allowed transition is higher than that of forbidden transitions. The fluorescence of Eu^{2+} and Mn^{2+} co-activated phosphors has been studied extensively, while the resonance-type energy-transfer (ET) mechanism between Eu^{2+} and Mn^{2+} has been extensively investigated in phosphate, borate, aluminate and silicate phosphors, such as $SrZn_2(PO_4)_2$[8], $(Ca,Mg,Sr)_9Y(PO_4)_7$[9], $Ba_2Ca(B_3O_6)_2$[10], $Ba_2Mg(BO_3)_2$[11], $BaMgAl_{10}O_{17}$[12] and $BaMg_2Al_6Si_9O_{30}$[13], because of their dipole-dipole interactions. The emission and excitation spectra of Eu^{2+} comprise the broad band because of the transitions from $4f^7$ ground state and $4f^65d$ excited state, while the emission of Mn^{2+} arises from the transition $^4T_1 \rightarrow {}^6A_1$[14]. Generally, the singly doped Mn^{2+} phosphor shows the weak red emission, while Eu^{2+} can serve as an efficient sensitizer. Ternary silicate-hosted phosphors have the advantages of stable crystal structure and high physical stability. Recently, we reported our study on a silicate-hosted, Eu^{2+} and Mn^{2+} co-activated, $A_3MgSi_2O_8$ (*A*MS, *A*=Ba, Ca and Sr) phosphor with an emitting band that covers the PAS for bio-illumination[15]. An Eu^{2+} luminescence of subsolidus phases bound by $Ba_3MgSi_2O_8$, $Ca_3MgSi_2O_8$ and $Sr_3MgSi_2O_8$ was reported by Barry[16]. Fluorescence of Eu^{2+} and Mn^{2+} co-activated in an *A*MS host has already been shown by Blasse[17]. However, many researchers have claimed to estimate the critical distance in certain phosphors without any adjustment. In the *A*MS-hosted phosphors, it is well known that Eu^{2+} occupies the lattice sites of *A* (*A* = Ba, Ca and Sr), while Mg^{2+} is replaced by Mn^{2+}[18]. It is critical to shorten the distance between cation *A* and Mg^{2+}, which would significantly improve the ET efficiency between Eu^{2+} and Mn^{2+}.

In this paper, we propose a solid-solution-phase phosphor synthesized by the conventional solid-state reduction method. The ET efficiency is optimized by the incorporation of Ca, and both ET and temperature-dependent properties are enhanced. This phosphor is found to be a promising material for biological illumination.

* This work has been supported by the National Natural Science Foundation of China (No.21076161).

** E-mail: djwang@tjut.edu.cn

Samples of powder with the formula $Ba_{1.75}Ca_{1.25}MgSi_2O_8$: xEu^{2+}, yMn^{2+} (BCMS: EM, x and y are denoted in atomic fraction) were prepared by high-temperature solid-state synthesis. Chemicals of $CaCO_3$ (99.99%, Aladdin, China), $BaCO_3$ (99.99%, Aladdin), MgO (99.99%, Aladdin), SiO_2 (99.99%, Aladdin) and Eu_2O_3 (99.99%, Aladdin) were mixed thoroughly using an agate mortar for 1 h and then fired in a temperature range of 1 300–1 400 °C in a weak reducing atmosphere of H_2 (8%) and N_2 (92%) for 3 h. The crystallographic data of the samples were collected on an X-ray powder diffractometer (Rigaku RINT Ultima-III, Japan) with a graphite monochromator using Cu Kα radiation (λ=0.154 062 nm), operating at 40 kV and 40 mA. Photoluminescence (PL) and photoluminescence excitation (PLE) spectra of the samples were recorded on a fluorescence spectrometer equipped with a 350 nm Xe flash lamp (Hitachi F-4500, Japan), and the excitation and emission slits were both set to be 2.5 nm. The temperature-dependent PL spectrum was recorded on a fluorescence spectrometer equipped with a 350 nm Xe flash lamp (Everfine Co. Ltd., EX-1000, China) and a 450 W xenon lamp for excitation.

Fig.1(a) shows the distance between the ions Ba^{2+}(Ca^{2+}) and Mg^{2+} for different cationic placeholders. Fig.1(b) and (c) show the crystal structures with SiO_4 tetrahedra for $Ba_3MgSi_2O_8$ and $Ca_3MgSi_2O_8$, respectively. In the $A_3MgSi_2O_8$ (A=Ba and Ca) host, Mg^{2+} was substituted by Mn^{2+} efficiently, and Ba^{2+} (Ca^{2+}) was replaced by Eu^{2+}, which is generally because of the similar ionic radii in the case of the Eu^{2+} and Mn^{2+} co-dopants. The ion distances are 3.638 2, 3.670 3 and 3.531 2 for Ba1, Ba2 and Ba3 of $Ba_3MgSi_2O_8$, respectively, and 3.386 1, 3.267 2 and 3.327 8 for Ca1, Ca2 and Ca3 of $Ca_3MgSi_2O_8$, respectively. Even though these two hosts are different, i.e., $Ba_3MgSi_2O_8$ is trigonal while $Ca_3MgSi_2O_8$ is monoclinic, both $Ba_3MgSi_2O_8$ and $Ca_3MgSi_2O_8$ belong to the merwinite family and the lattice of each is formed by SiO_4 tetrahedra layers. The structural information for $Ca_3MgSi_2O_8$ and $Ba_3MgSi_2O_8$ was obtained from the inorganic crystal structure database (ICSD) and the study of Cheol-hee Park[19], respectively. By comparing their basic unit cells, we find that their structures with SiO_4 tetrahedra are similar, which provide a structural basis for the solid solution. The ET efficiency is closely related to the distance between the sensitizer and activator, namely the distance between Eu^{2+} and Mn^{2+} for the $A_3MgSi_2O_8$ (A=Ba and Ca) host. As the distance between Ca^{2+} and Mg^{2+} is shorter than that between Ba^{2+} and Mg^{2+}, we propose a way to improve the ET efficiency by establishing a solid solution of $Ba_{1.7}Ca_{1.25}Mg_{1-x}Si_2O_8$: 0.05Eu^{2+}, xMn^{2+} to shorten the distance between Eu^{2+} and Mn^{2+}. Fig.1(d) shows the XRD patterns of $Ba_{3-x}Ca_xMgSi_2O_8$. The lattice parameters of pure $Ba_3MgSi_2O_8$ are a=0.972 41 nm, c=0.727 65 nm and c/a=0.748 3, and those of $Ca_3MgSi_2O_8$ are a=1.325 4 nm, b=0.529 3 nm, c=0.932 8 nm, with lattice parameters of intermediate compositions varying linearly according to the Végard law.

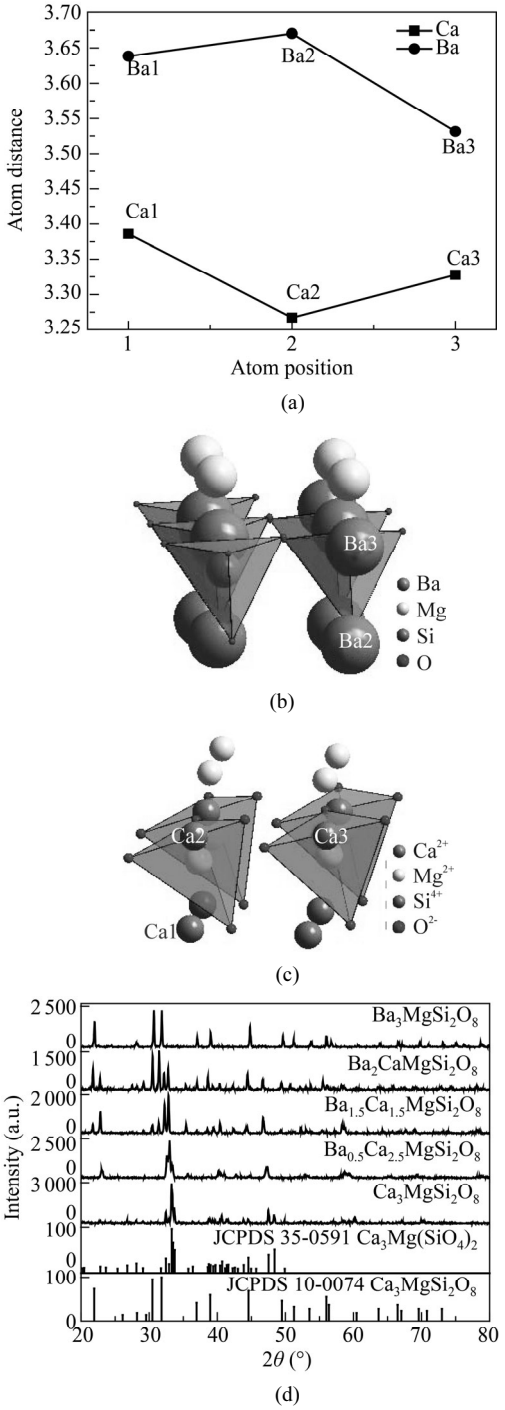

Fig.1 (a) Ion distances between Ba^{2+} (Ca^{2+}) and Mg^{2+} for different cationic placeholders; Crystal structures with SiO_4 tetrahedra for (b) $Ba_3MgSi_2O_8$ and (c) $Ca_3MgSi_2O_8$; (d) XRD patterns of $Ba_{3-x}Ca_xMgSi_2O_8$

Fig.2(a) shows the PL spectra of the $Ba_{1.7}Ca_{1.25}Mg_{1-x}Si_2O_8$: 0.05Eu^{2+}, xMn^{2+} samples, and the inset of Fig.2(a) shows the dependence of Mn^{2+} content on the PL intensity ratio of red to blue light. Once the proper composition of Ba–Ca is fixed, it is possible to obtain a phosphor

with red peaks at certain positions irrespective of changes to the Mn^{2+} doping content. The PL intensity of Eu^{2+} is decreased monotonically with the increase of Mn^{2+} content from 0 mol to 0.2 mol, whereas that of Mn^{2+} is increased distinctly at the beginning before reaching a maximum owing to the quenching effect. The PL intensity ratio of red to blue emissions shows that the energy transfer from Eu^{2+} to Mn^{2+} approaches a constant. Fig.2(b) shows the calculation result of ET efficiency for $Ba_{1.7}Ca_{1.25}Mg_{1-x}Si_2O_8$: $0.05Eu^{2+}$, $0.1Mn^{2+}$. The critical distance between Eu^{2+} and Mn^{2+}, defined as R_c, can be estimated using Blasse's relation as

$$R_c \approx 2\left(\frac{3V}{4\pi X_c N}\right)^{1/3}, \quad (1)$$

where V is the volume of the unit cell, N is the number of the host cations in the unit cell, and X_c is the critical concentration for R_c. For the host $Ba_3MgSi_2O_8$, N=38, V=0.595 87 nm^3 and X_c=0.7%, where the concentration effect begins to emerge, and R_c is computed to be 0.349 8 nm. We then obtain the critical distance of $Ca_3MgSi_2O_8$ in the same way, where N=26, V=0.654 03 nm^3, X_c=0.7%, and R_c is 0.409 5 nm. The critical distance of $Ca_3MgSi_2O_8$ is much longer than that of $Ba_3MgSi_2O_8$, which provides direct evidence that the incorporation of Ca^{2+} may improve the ET efficiency from Eu^{2+} to Mn^{2+} in the $Ba_{3-x}Ca_xMgSi_2O_8$ host. It is generally accepted that in the ET process, Eu^{2+} is the effective sensitizer in the energy absorption while Mn^{2+} is the activator responsible for the red emission. Therefore, we could assume that in the single-direction energy transfer from Eu^{2+} to Mn^{2+}, its absorption energy is a constant. Based on this assumption, we quantitatively assess the ET efficiency of our sample. The following equation is used to calculate the ET efficiency:

$$\eta_{et} = 1 - \frac{\int \Delta A_{Blue} dA - \int \Delta A_{red} dA}{\int \Delta A_{Blue} dA}, \quad (2)$$

where $\int \Delta A_{Blue} dA$ and $\int \Delta A_{red} dA$ are the blue and red differential integral areas shown in the shadow areas of the blue and red parts, respectively. The ET efficiency is found to increase with the increase of concentration. At x=0.1, the efficiency is approximately 76% for the Eu^{2+}, Mn^{2+} co-activated samples, indicating preferred energy transfer among the dopants.

Fig.3 shows the diffuse reflection spectra (DRS) of the as-fired phosphor samples with compositions of $Ba_{1.7}Ca_{1.25}Mg_{1-x}Si_2O_8$: $0.05Eu^{2+}$, xMn^{2+}, where x=0.05, 0.06, 0.08 and 0.10. The DRS of $Ba_{1.7}Ca_{1.25}Mg_{1-x}Si_2O_8$: $0.05Eu^{2+}$, xMn^{2+} consist of several strong absorption bands at 290 nm, 350 nm and 400 nm, respectively, owing to electronic transition absorption of Eu^{2+} in $^8S_{7/2} \rightarrow {}^2t_{2g}$. The broad absorption band positioned from 310 nm to 400 nm is ascribed to the $4T^1(^4G) \rightarrow {}^6A_1(^6S)$ electronic transition absorption. The similarity in absorption patterns of the samples indicates that our assumption is reasonable.

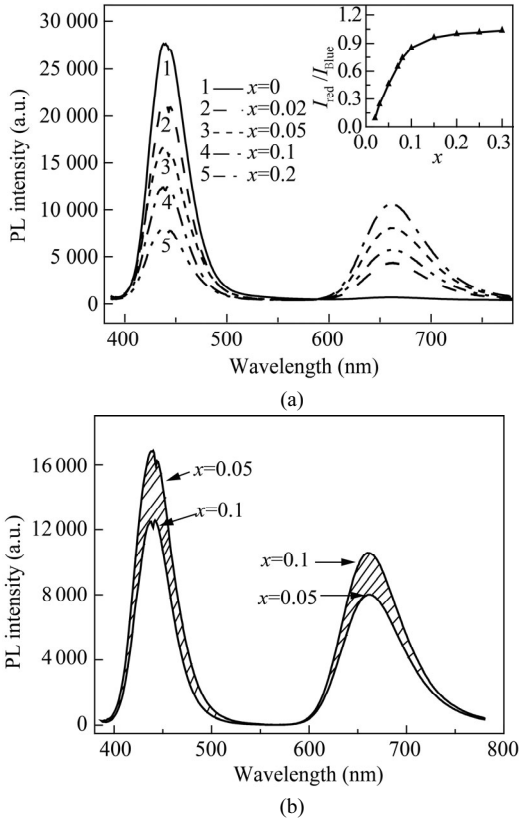

Fig.2 (a) PL spectra of the $Ba_{1.7}Ca_{1.25}Mg_{1-x}Si_2O_8$: $0.05Eu^{2+}$, xMn^{2+} samples (The inset is Mn^{2+}-content dependence of the PL intensity ratio of red to blue light.); (b) Calculation results of ET efficiency for $Ba_{1.7}Ca_{1.25}Mg_{0.9}Si_2O_8$: $0.05Eu^{2+}$, $0.1Mn^{2+}$

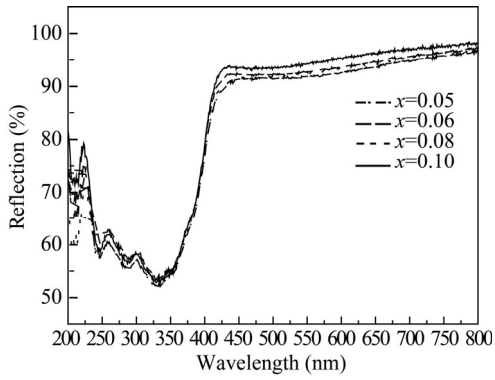

Fig.3 DRS of $Ba_{1.7}Ca_{1.25}Mg_{1-x}Si_2O_8$: $0.05Eu^{2+}$, xMn^{2+}, where x=0.05, 0.06, 0.08 and 0.10

An overlap in the spectra is observed between PL of Eu^{2+} and the enlarged PLE of Mn^{2+} in Fig.4, which indicates that a prerequisite level of energy transfer from Eu^{2+} to Mn^{2+} is met. The broad-band PLE of Eu^{2+}, covering the wavelength range from 250 nm to 400 nm, exhibits the strong absorption of UV light. This excitation band corresponds to the electronic transition absorption of $^8S_{7/2} \rightarrow {}^2t_{2g}$ for Eu^{2+}. The blue band results from the $4f^65d^1 \rightarrow 4f^7$ transition of Eu^{2+}, while the red band results

from the spin-forbidden $^4T_1(^4G) \rightarrow {}^6A_1(^6S)$ transition of Mn^{2+}. The excitation spectrum of Mn^{2+} contains five bands at about 280 nm, 330 nm, 380 nm, 470 nm and 560 nm, which may be ascribed to the transitions of energy levels from $^6A_1(^6S)$ to $^4E(^4D)$, $^4T_2(^4D)$, [$^4A_1$ (^4G), $^4E(^4G)$], $^4T_2(^4G)$ and $^4T_1(^4G)$, respectively, for Mn^{2+}.

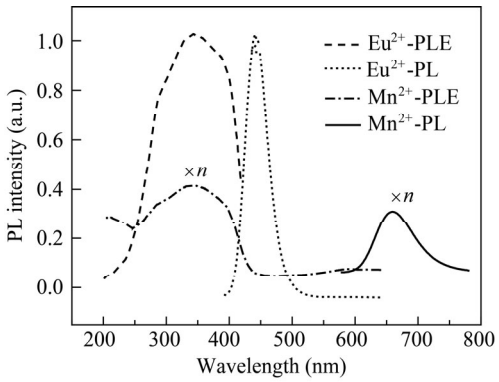

Fig.4 PLE and PL spectra of $Ba_{1.7}Ca_{1.25}MgSi_2O_8$: $0.05Eu^{2+}$ and $Ba_{1.75}Ca_{1.25}Mg_{0.9}Si_2O_8$: $0.1Mn^{2+}$

Fig.5 shows the temperature-dependent quantum efficiencies of $Ba_{1.7}Ca_{1.25}Mg_{0.9}Si_2O_8$: $0.05Eu^{2+}$, $0.1Mn^{2+}$, $Ba_{0.95}Ca_2Mg_{0.9}Si_2O_8$: $0.05Eu^{2+}$, $0.1Mn^{2+}$, $Ba_{2.95}Mg_{0.9}Si_2O_8$: $0.05Eu^{2+}$, $0.1Mn^{2+}$ and $Ca_{2.95}Mg_{0.9}Si_2O_8$: $0.05Eu^{2+}$, $0.1Mn^{2+}$. $Ba_{1.7}Ca_{1.25}Mg_{0.9}Si_2O_8$: $0.05Eu^{2+}$, $0.1Mn^{2+}$ shows the highest thermal stability because of effective incorporation of Ba^{2+} into the crystal structure of the Ba–Ca solid-solution host. The intensities are decreased to 76.3%, 66.2%, 57.7% and 45.2% of the initial values at 220 nm for the $Ba_{1.7}Ca_{1.25}Mg_{0.9}Si_2O_8$: $0.05Eu^{2+}$, $0.1Mn^{2+}$, $Ba_{0.95}Ca_2Mg_{0.9}Si_2O_8$: $0.05Eu^{2+}$, $0.1Mn^{2+}$, $Ba_{2.95}Mg_{0.9}Si_2O_8$: $0.05Eu^{2+}$, $0.1Mn^{2+}$ and $Ca_{2.95}Mg_{0.9}Si_2O_8$: $0.05Eu^{2+}$, $0.1Mn^{2+}$ samples, respectively. The Ba–Ca solid solution serves as a guide for proper selection of compositions of Ba–Ca in $(Ba,Ca)_3MgSi_2O_8$ to achieve the desired properties under specific operating temperatures or different packaging modes in service.

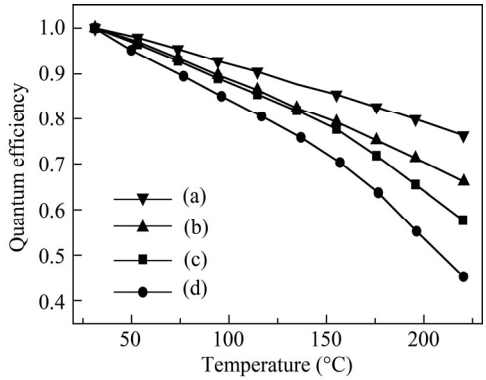

Fig.5 Temperature-dependent quantum efficiencies of (a) $Ba_{1.7}Ca_{1.25}Mg_{0.9}Si_2O_8$: $0.05Eu^{2+}$, $0.1Mn^{2+}$, (b) $Ba_{0.95}Ca_2Mg_{0.9}Si_2O_8$: $0.05Eu^{2+}$, $0.1Mn^{2+}$, (c) $Ba_{2.95}Mg_{0.9}Si_2O_8$: $0.05Eu^{2+}$, $0.1Mn^{2+}$ and (d) $Ca_{2.95}Mg_{0.9}Si_2O_8$: $0.05Eu^{2+}$, $0.1Mn^{2+}$

A BCMS: EM phosphor with enhanced ET efficiency and improved temperature-dependent quantum efficiency is synthesized. Phase analysis reveals a solution phase. The PLE and PL spectra of $Ba_{1.7}Ca_{1.25}MgSi_2O_8$: $0.05Eu^{2+}$ and $Ba_{1.75}Ca_{1.25}Mg_{0.9}Si_2O_8$: $0.1Mn^{2+}$ demonstrate the ET from Eu^{2+} to Mn^{2+}. Furthermore, we also propose that the $Ba_{1.7}Ca_{1.25}Mg_{1-x}Si_2O_8$: $0.05Eu^{2+}$, xMn^{2+} phosphor can be tuned to match the PAS with various red to blue light ratios.

References

[1] Andreiadis E. S., Chavarot-Kerlidou M., Fontecave M. and Artero V., Photochemistry Photobiology **87**, 946 (2011).

[2] Ge Zhua, Yuhua Wang, Zhipeng Ci, Bitao Liu, Yurong Shi and Shuangyu Xin, Journal of Electrochemical Society **158**, J236 (2011).

[3] Xue Y. N., Xiao F. and Zhang Q. Y., Spectrochimica Acta Part A: Molecular and Biomolecular Spectroscopy **78**, 1445 (2011).

[4] Huang C. H., Kuo T. W. and Chen T. M., ACS Applied Materials & Interfaces **2**, 1395 (2010).

[5] Yang Bin, Zhang Yue-pin, Xu Bo and Xia Hai-ping, Optoelectronics Letters **9**, 30 (2013).

[6] Dai Xiu-hong, Li Hong-lian, Pang Li-bin and Gao Shao-jie, Optoelectronics Letters **9**, 194 (2013).

[7] Wang Pei-yuan, Xia Hai-ping, Peng Jiang-tao, Hu Hao-yang, Tang Lei, Zhang Yue-pin, Chen Bao-jiu and Jiang Hao-chuan, Optoelectronics Letters **9**, 285 (2013).

[8] Yi L., Zhou L., Gong F., Lan Y., Tong Z. and Sun J., Materials Science and Engineering: B **172**, 132 (2010).

[9] Huang C.-H., Wu P.-J., Lee J.-F. and Chen T.-M., Journal of Materials Chemistry **21**, 10489 (2011).

[10] Xiao F., Xue Y. N., Ma Y. Y. and Zhang Q. Y., Physica B: Condensed Matter **405**, 891 (2010).

[11] Yuan S., Yang Y., Zhang X., Tessier F., Cheviré F., Adam J.-L., Moine B. and Chen G., Optics Letters **33**, 2865 (2008).

[12] Moon T., Hong G. Y., Lee H.-C., Moon E.-A., Jeoung B. W., Hwang S.-T., Kim J. S. and Ryu B.-G., Electrochemical and Solid-State Letters **12**, J61 (2009).

[13] Wei Lü, Zhendong Hao, Xia Zhang, Yongshi Luo, Xiaojun Wang and Jiahua Zhang, Inorganic Chemistry **50**, 7846 (2011).

[14] Mengmeng Shang, Guogang Li, Dongmei Yang, Xiaojiao Kang, Chong Peng, Ziyong Cheng and Jun Lin, Dalton Transactions **40**, 9379 (2011).

[15] Qi-fei Lu, Jian Lia and Da-jian Wang, Current Applied Physics **13**, 1506 (2013).

[16] Barry T. L., J. Electrochem. Soc: Solid State Science **115**, 733 (1968).

[17] Blasse G., Wanmaker W. L., Tervrugt J. W. and Bril A., Philips Res. Repts. **23**, 189 (1968).

[18] Ma L., Wang D., Mao Z., Lu Q. and Zhao Z., Applied Physics Letters **93**, 144101 (2008).

[19] Park C. H., Hong S. T. and Keszler D. A., Journal of Solid State Chemistry **182**, 496 (2009).